nature portfolio

Peer Review File

Stabilization of sliding ferroelectricity through exciton condensation

Corresponding Author: Dr Massimo Rontani

Parts of this Peer Review File have been redacted as indicated to remove third-party material.

This file contains all reviewer reports in order by version, followed by all author rebuttals in order by version.

Version 0:

Reviewer comments:

Reviewer #1

(Remarks to the Author)
This paper presents a theoretical study on the role of exciton condensation in stabilizing sliding ferroelectricity in bilayer WTe_2. By proposing that electron-hole (e-h) interactions and the formation of an excitonic insulator (EI) phase significantly renormalize the sliding energy barrier, the work offers a novel and physically insightful mechanism. The concept of coupling between excitonic order and ferroelectricity in a van der Waals (vdW) bilayer is highly innovative and of potential broad interest to the communities working on 2D sliding ferroelectrics and correlated electronic states. It is an interesting piece of a thorough study that merits due consideration for its publication upon moderate revision.

Comment 1: To ensure that the data in the paper can be reproduced, please provide models with sufficiently detailed parameters in the supplementary materials, including the four-band model and exciton insulator model. The authors should also compare their four-band model band structure with the DFT results.

Comment 2: The 2D polarizability α_2D is a critical parameter for the Rytova-Keldysh potential (as shown in Supplementary Fig. 2). The value of 4.3 is used without justification. How was this value determined or estimated? A sensitivity analysis or a justification based on the electronic properties of bilayer WTe_2 (e.g., from the DFT dielectric function) is essential to assess the robustness of the predicted gap and energy barrier.

Comment 3: How do we understand that Egap decreases with increasing α2D in Supplementary Figure 2?

Comment 4: As far as I know, the ferroelectric switching barrier of different material is not related to the ferroelectric Curie temperature. For example, the ferroelectric sliding barrier is only a few meV in sliding ferroelectrics, but the FE order is stable at room temperature. Therefore, I do not think the author's simple estimate of 70 K is meaningful. Likewise, I don't understand the significance of the author's analogy with BCS model.

Comment 5: Could the authors discuss how exciton contributions affect sliding ferroelectric semiconductors?

(Remarks on code availability)

Reviewer #2

(Remarks to the Author)
In this manuscript, the authors construct a model to investigate the impact of excitonic effects on the electronic structure and energy during the sliding process of WTe2 bilayers. Their results reveal that excitonic effects open a significant bandgap in WTe2 bilayers, leading the system to transition towards an excitonic insulator (EI) phase. This explains the experimentally observed Curie temperature, which is higher than predicted by density functional theory (DFT). While the work presents intriguing findings, several critical aspects require deeper exploration and substantial revisions to strengthen the manuscript for publication.

1. When discussing the excitonic effect in the manuscript, the value $\alpha_2 D = 4.3$ Å appears. Could you please explain the origin of this data? Additionally, the text describes that $\alpha_2 D = 4.3$ Å opens a 3 meV energy gap in the energy band of GMS. Is this 3 meV energy gap reflected in the figure?
2. The manuscript mentions that the excitonic contribution is widespread in general two-dimensional systems. It is suggested to list the potential impacts of exciton in other studies to further reveal the research directions of excitonic effect in two-dimensional systems.
3. The author discussed the influence of the excitonic effect on the band structure of bilayer WTe_2 while neglecting SOC (Spin-Orbit Coupling). Could you please explain whether there is an interaction between the excitonic effect and SOC? Additionally, how would the band structure change if SOC is considered in the author's model?
4. In the experimental study of the sliding ferroelectricity of WTe2 bilayers, the properties of WTe2 bilayers at different temperatures were investigated. Is there an impact of temperature on the excitonic effect?
5. The manuscript employs a model to discuss the electronic properties of WTe2 bilayers under the excitonic effect. Have these properties been compared with other experimental or theoretical works? Could additional analysis be provided?

(Remarks on code availability)

Reviewer #3

(Remarks to the Author)
Excitons in TMDs have been known for a while. Connection with sliding ferroelectrics appears interesting. The manuscript by Rontani et al. reports the energy gain from exciton condensation in bilayer WTe_2 and concludes that this condensation plays a critical role in stabilizing its sliding ferroelectricity. The data and logic presented are clear and accessible. However, the listed critical issues below must be satisfactorily addressed before I can reconsider my evaluation:

1) Unlike in conventional bulk ferroelectrics, the calculated energy barrier separating two polarized structures does not serve as a definitive indicator of ferroelectric stability in sliding ferroelectrics. For example, bilayer BN—with an energy barrier of only ~2 meV/f.u.—remains stable well above room temperature (see Refs. 6 and 42), despite this barrier being significantly smaller than the thermal energy at 300 K. A continuum model from Bauer's group further suggests that WTe_2 bilayers may exhibit a Curie temperature as high as 660 K with a sub-meV barrier (Phys. Rev. Lett. 130, 176801), which does not take exciton correction into consideration. Experimentally, stability can be strongly influenced by other factors such as boundaries, domain walls, etc. Thus, attributing the stability of sliding ferroelectricity in bilayer WTe_2 observed in experiments primarily to exciton condensation lacks solid scientific justification.

2) According to the authors'data, the exciton binding energy is on the order of tens of meV, implying that exciton condensation can be readily disrupted and depopulated by thermal excitation at room temperature. It is therefore quite questionable to claim that excitons are responsible for the ferroelectric stability of bilayer WTe_2 around room temperature.

3) Figure 4 presents a corrected double-well potential profile. What are the polarization values at the corrected minima, and how well do they align with experimental measurements? Such comparison can make the data in the manuscript more convincing.

(Remarks on code availability)

Reviewer #4

(Remarks to the Author)
In their manuscript, D'Alessio et al. investigate the excitonic effects in sliding ferroelectric bilayer WTe_2. They propose that (i) excitonic effects induce significant energy band renormalizations in the ground state, and (ii) exciton condensation helps stabilize ferroelectricity upon sliding, beyond previous predictions.

Regarding point (i), the reported band renormalizations appear reasonable for bilayer WTe_2, given its small bandgap. However, such effects may not be generalizable to other sliding ferroelectrics, such as MoS_2, which possesses a larger bandgap.

As for point (ii), the high Curie temperature can be adequately explained by molecular dynamics simulations using machine-learned force fields, which do not incorporate any excitonic effects.

While excitonic effects may play a role in narrow-gap or metallic sliding ferroelectric systems, I believe they are unlikely to be the key factor in stabilizing the ferroelectric state. Therefore, in my view, the manuscript in its current form may not be suitable for publication in Nature Communications.

(Remarks on code availability)

Version 1:

Reviewer comments:

Reviewer #1

(Remarks to the Author)
The author's response generally addressed my concerns. I believe this work is important for understanding the sliding ferroelectric problem in narrow-bandgap (or semimetallic) layered materials, and its conclusions are appropriate; therefore, I recommend the paper be accepted.

The author provided details about the method and offered code for verification, greatly enhancing the reproducibility. In the end, before publication, please add the details on how to obtain the "phonon" parameter δH1 via "y" in the the supplementary materials.

(Remarks on code availability)

Reviewer #2

(Remarks to the Author)
Having reviewed the reply, I accept the paper for publication in its current form.

(Remarks on code availability)

Reviewer #3

(Remarks to the Author)
After carefully considering the authors' responses, the central concern raised in the original review remains unresolved. As I understand it, the claimed novelty of the manuscript—as suggested by its title—rests on the assertion that exciton condensation induces a substantial renormalization of the interlayer sliding barrier in bilayer WTe_2, thereby enabling robust sliding ferroelectricity at room temperature. This claim is motivated by the fact that, in the absence of excitonic effects, the intrinsic sliding barrier is on the sub-meV scale. However, neither the revised manuscript nor the authors' responses provide convincing or quantitative evidence to substantiate this proposed mechanism.
As emphasized in the previous review, the magnitude of the sliding barrier enhanced by exciton condensation is not a determining factor for the existence or stability of sliding ferroelectricity itself. Instead, it is primarily an indicator of the switching characteristics under an external electric field. Existing experimental and theoretical studies have already established that sliding ferroelectricity in WTe_2 is highly robust at and below room temperature, despite the intrinsically small (sub-meV) barrier. The excitonic effect in this material is not as important as claimed in the stabilization of ferroelectricity. Furthermore, the influence of exciton condensation is expected to be relevant only at low temperatures. Although the exciton binding energy in WTe_2 is relatively large (on the order of ~270 meV), exciton condensation has been reported to occur at much lower temperatures, around 100 K (see, e.g., Refs. 52 and 53). This significantly limits the temperature window in which excitonic effects can meaningfully contribute to the ferroelectric behavior, particularly at/near room temperature.
Given these considerations, the overall scientific contribution of the manuscript requires reassessment. In its present form, the work does not convincingly demonstrate a level of novelty or impact commensurate with the standards required for publication in Nature Communications.

(Remarks on code availability)

Reviewer #4

(Remarks to the Author)
I have read the authors' reply. It seems my understanding on the manuscript is right.
The novelty of this manuscript is to propose "exciton effects renormalize the sliding barrier". I think it does not play the key role in the stabilizing the ferroelectricity. Nevertheless I cannot judge whether the novelty and importance meet the standard of Nat. Comm. or not; I therefore suggest the editor to find one more referee to judge its novelty and importance.

(Remarks on code availability)

Version 2:

Reviewer comments:

Reviewer #3

(Remarks to the Author)
I would like to acknowledge the authors' efforts in addressing the concerns I raised. The revised data and figures partially alleviate my previous concerns; however, I remain skeptical regarding the plausibility of coherent excitonic condensation around room temperature(which is the key factor in reshaping the barrier claimed in the manuscript), even after reviewing their responses.
Nevertheless, the revised manuscript highlights a potentially significant effect—namely, the reshaping of sliding ferroelectricity in bilayer WTe_2 due to excitonic condensation—an aspect that had been previously overlooked in discussions of the material's ferroelectric properties.
I am OK with the publication of the revised manuscript in its current form.

(Remarks on code availability)

Reply to reviewers

January 8, 2026

We thank the Reviewers for their constructive criticisms as well as for their time spent in the review process. In the following, we address all of their comments point by point. For ease of reference we reproduce here the review reports in *Italics*. Our responses are in Roman font. The changes in the manuscript are highlighted in red.

Reviewer # 1

This paper presents a theoretical study on the role of exciton condensation in stabilizing sliding ferroelectricity in bilayer WTe2. By proposing that electron-hole (e-h) interactions and the formation of an excitonic insulator (EI) phase significantly renormalize the sliding energy barrier, the work offers a novel and physically insightful mechanism. The concept of coupling between excitonic order and ferroelectricity in a van der Waals (vdW) bilayer is highly innovative and of potential broad interest to the communities working on 2D sliding ferroelectrics and correlated electronic states. It is an interesting piece of a thorough study that merits due consideration for its publication upon moderate revision.

Reviewer 1: *Comment 1: To ensure that the data in the paper can be reproduced, please provide models with sufficiently detailed parameters in the supplementary materials, including the four-band model and exciton insulator model. The authors should also compare their four-band model band structure with the DFT results.*

Authors Reply: We have substantially extended the Supplementary Information (SI), to ensure that the data in the paper can be reproduced. We now provide a detailed description of both the four-band model and the self-consistent calculation of the excitonic insulator phase, including all relevant parameters, in Supplementary Section I. In addition, we explicitly compare the band structure obtained from the four-band model with the corresponding DFT results, as shown in Supplementary Figure 3. The parts of the SI concerning these points are reported below.

I. FOUR-BAND MODEL

We develop the four-band model mentioned in the main text to investigate the onset of macroscopic excitonic coherence in bilayer WTe_2, as a function of the relative sliding of the two layers, y. This model fully complies with the space group symmetry of the bilayer for all y, in the absence of e-h interaction, and provides a transparent picture of the orbital character of the exciton wave function. This allows us to analyze the breaking of microscopic symmetries due to exciton condensation.

A. Noninteracting Hamiltonian

Within the envelope function approximation, the model provides the two lowest conduction (c) and two highest valence (v) bands by spanning the Hilbert space through a four-dimensional orbital basis. In this representation, the $\boldsymbol{k}$-resolved noninteracting Hamiltonian, $\hat{H}(\boldsymbol{k})$, is a 4×4 matrix. The basis is made of the Bloch states at Γ obtained *ab initio* for the *glide-mirror symmetric* (GMS) configuration ($y=0$), after a rotation. The non rotated states, plotted in Supplementary Fig. 1b, are either even or odd with respect to the symmetry operations of the space group, i.e.: (i) the glide-mirror operation, $\mathbb{G}$, a combination of mirror reflection $z\to-z$ and half-period translation $y\to y+b/2$ along the y axis (b is the lattice constant along y); (ii) the mirror reflection $x\to-x$, $\mathbb{M}$, with the vertical mirror plane yz intersecting the row of W atoms at the origin.

As apparent from Supplementary Fig. 1b, the Bloch states symmetrically spread between the two layers. Since we are interested in the charge transfer and consequent asymmetry between layers, we rotate the basis frame to introduce a layer index, σ_z, as the eigenvalue of the 2×2 z-component Pauli matrix, $\hat{\sigma}_z$, with eigenvectors $|\chi^{\pm}_{\sigma_z}\rangle$ obeying $\hat{\sigma}_z|\chi^{\pm}_{\sigma_z}\rangle=\pm|\chi^{\pm}_{\sigma_z}\rangle$. Here the pseudospinors $|\chi^{+}_{\sigma_z}\rangle$ and $|\chi^{-}_{\sigma_z}\rangle$ are linear combinations of (either conduction or valence) Bloch states, and are localized respectively in the top and bottom layer. Furthermore, as the $\mathbb{M}$ symmetry survives for $y\neq0$, we introduce a second orbital pseudospin, τ_z, corresponding to orbitals respectively even ($\tau_z=+1$, top row of Supplementary Fig. 1b) or odd ($\tau_z=-1$, bottom row) under reflection, i.e., $\hat{\tau}_z|\chi^{\pm}_{\tau_z}\rangle=\pm|\chi^{\pm}_{\tau_z}\rangle$. The complete basis set stems from the external product of the two pseudospinors, $|\chi^{\pm}_{\sigma_z},\chi^{\pm}_{\tau_z}\rangle\equiv|\chi^{\pm}_{\sigma_z}\rangle\otimes|\chi^{\pm}_{\tau_z}\rangle$. In this representation, the symmetry operations are

$$\mathbb{G}=\hat{\sigma}_x\otimes\mathbb{I}_\tau\,,\quad \mathbb{M}=\mathbb{I}_\sigma\otimes\hat{\tau}_z\,, \tag{1}$$

where $\mathbb{I}_\sigma$ and $\mathbb{I}_\tau$ are the 2×2 unit matrices in the layer and orbital pseudospin spaces, respectively.

The eigenvalues of the noninteracting Hamiltonian for $y=0$, $\hat{H}_0(\boldsymbol{k})$, are—by construction—the DFT energy bands of the GMS structure, $\varepsilon^0_{M,G}(\boldsymbol{k})$, with the subscripts $M=\pm$ and $G=\pm$ labeling the parity of the corresponding eigenvector with respect to $\mathbb{M}$ and $\mathbb{G}$ operations, respectively. The explicit form of $\hat{H}_0(\boldsymbol{k})$ is

$$\begin{aligned}\hat{H}_0(\boldsymbol{k})=&\left(\frac{\mathbb{I}_\sigma+\hat{\sigma}_x}{2}\right)\otimes\left(\frac{\mathbb{I}_\tau+\hat{\tau}_z}{2}\right)\varepsilon^0_{+,+}(\boldsymbol{k})+\left(\frac{\mathbb{I}_\sigma-\hat{\sigma}_x}{2}\right)\otimes\left(\frac{\mathbb{I}_\tau+\hat{\tau}_z}{2}\right)\varepsilon^0_{+,-}(\boldsymbol{k})+\\&\left(\frac{\mathbb{I}_\sigma+\hat{\sigma}_x}{2}\right)\otimes\left(\frac{\mathbb{I}_\tau-\hat{\tau}_z}{2}\right)\varepsilon^0_{-,+}(\boldsymbol{k})+\left(\frac{\mathbb{I}_\sigma-\hat{\sigma}_x}{2}\right)\otimes\left(\frac{\mathbb{I}_\tau-\hat{\tau}_z}{2}\right)\varepsilon^0_{-,-}(\boldsymbol{k})\,.\end{aligned} \tag{2}$$

The energy bands are plotted in Supplementary Fig. 1a and c respectively along the ΓX cut and in the rectangular sector of the Brillouin zone $k_x\in[0,0.35]$, $k_y\in[-0.1,0.1]$.

For finite displacement y, we add to the total Hamiltonian, $\hat{H}(\boldsymbol{k})=\hat{H}_0(\boldsymbol{k})+\hat{H}_1$, the term $\hat{H}_1$, which is the interaction between the electron and the "frozen" phonon corresponding to the rigid sliding of the two layers,

$$\hat{H}_1=(\hat{\sigma}_z\otimes\mathbb{I}_\tau)\,\delta_{H_1}\,. \tag{3}$$

Here the "phonon" parameter δ_{H_1} depends explicitly on y. The term (3) breaks the glide-mirror symmetry, as it does not commute with $\mathbb{G}$, and explicitly accounts for the layer polarization through the average value of $\langle\hat{\sigma}_z\rangle$ over the ground state.

B. Bethe-Salpeter equation and Coulomb interaction

Within the four-band model, the Bethe-Salpeter equation of motion for excitons that generalizes the expression (2) of the main text is

$$\sum_{v',c',\boldsymbol{k}'}H^{v'c'\boldsymbol{k}'}_{vc\boldsymbol{k}}\Psi_x^{v'c'\boldsymbol{k}'}=E_x\Psi_x^{vc\boldsymbol{k}}\,. \tag{4}$$

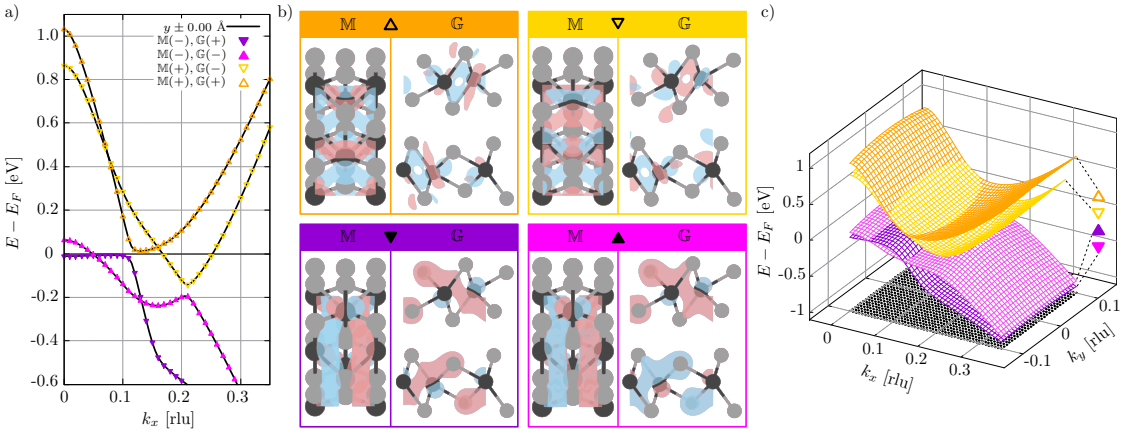

Supplementary Figure 1: **Orbital basis and symmetry.** a) Energy bands for the GMS structure along the ΓX cut of the Brillouin zone computed from density functional theory, as in Fig. 2 of the main text. The superimposed triangle symbols (open/filled and up/down) point to the symmetry classification of the states at Γ, tabulated in both legend and panel b. Since the glide-mirror symmetry is preserved along the ΓX line and there are no anticrossings, the symmetry labeling is extended to all $\boldsymbol{k}$ points, as the orbital character of each labeled band changes smoothly as one moves through the Brillouin zone. b) Wave functions (real part) at Γ of the highest two valence and lowest two conduction bands. The amplitude map colour points to the parity of the wave function with respect to mirror ($\mathbb{M}$) and glide-mirror ($\mathbb{G}$) symmetry operations, the red [blue] corresponding to the positive [negative] amplitude. In each one of the four panels, the left inset shows the top view of the bilayer (x axis in the horizontal direction) and the right inset shows the lateral view (y axis in the horizontal direction). Dark and light gray atoms are W and Te, respectively. c) Three-dimensional plot of the bands in a selected rectangular range of the Brillouin zone, illustrating the symmetry classification in the $\boldsymbol{k}$ space.

Now $\Psi_x^{vc\boldsymbol{k}}$ is the component of the exciton wave function that gives the probability amplitude for exciting an electron from the valence band v to the conduction band c, conserving the momentum $\boldsymbol{k}$. The indices v and c label two of the four energy bands derived from the solution of $\hat{H}_0 + \hat{H}_1$, as defined in (2) and (3). The kernel of (4) is

$$H_{vc\boldsymbol{k}}^{v'c'\boldsymbol{k}'} = \big[\varepsilon_c(\boldsymbol{k}) - \varepsilon_v(\boldsymbol{k})\big]\delta_{vv'}\,\delta_{cc'}\,\delta_{\boldsymbol{k}\boldsymbol{k}'} \;-\; W_{vc\boldsymbol{k}}^{v'c'\boldsymbol{k}'}\,, \tag{5}$$

and contains the screened electron-hole Coulomb attraction, W. Importantly, since the model provides us with the layer index σ_z for the eigenvectors of $\hat{H}_0(\boldsymbol{k}) + \hat{H}_1(\boldsymbol{k})$, we can generalize the form of the two-dimensional Rytova-Keldysh potential to the bilayer system [1]. Therefore, we resolve the Coulomb interaction matrix element, $W_{vc\boldsymbol{k}}^{v'c'\boldsymbol{k}'}$, as

$$\begin{aligned} W_{vc\boldsymbol{k}}^{v'c'\boldsymbol{k}'} = {} & W(\boldsymbol{k}-\boldsymbol{k}',0)\Big[\langle\psi_v^{\mathrm{T}}(\boldsymbol{k})|\psi_{v'}^{\mathrm{T}}(\boldsymbol{k}')\rangle\langle\psi_c^{\mathrm{T}}(\boldsymbol{k})|\psi_{c'}^{\mathrm{T}}(\boldsymbol{k}')\rangle^* + \langle\psi_v^{\mathrm{B}}(\boldsymbol{k})|\psi_{v'}^{\mathrm{B}}(\boldsymbol{k}')\rangle\langle\psi_c^{\mathrm{B}}(\boldsymbol{k})|\psi_{c'}^{\mathrm{B}}(\boldsymbol{k}')\rangle^*\Big] + \\ & W(\boldsymbol{k}-\boldsymbol{k}',h)\Big[\langle\psi_v^{\mathrm{T}}(\boldsymbol{k})|\psi_{v'}^{\mathrm{T}}(\boldsymbol{k}')\rangle\langle\psi_c^{\mathrm{B}}(\boldsymbol{k})|\psi_{c'}^{\mathrm{B}}(\boldsymbol{k}')\rangle^* + \langle\psi_v^{\mathrm{B}}(\boldsymbol{k})|\psi_{v'}^{\mathrm{B}}(\boldsymbol{k}')\rangle\langle\psi_c^{\mathrm{T}}(\boldsymbol{k})|\psi_{c'}^{\mathrm{T}}(\boldsymbol{k}')\rangle^*\Big]\,. \end{aligned} \tag{6}$$

Here $|\psi_i^{\mathrm{T}}(\boldsymbol{k})\rangle$ and $|\psi_i^{\mathrm{B}}(\boldsymbol{k})\rangle$ are the projections of the ith eigenvector ($i = c, v$) onto the top and bottom layer, respectively, and the screened interaction is

$$W(\boldsymbol{q},z) = \frac{e^2}{2\varepsilon_0 A}\,\frac{1}{q\,\epsilon(q,z)}\,, \tag{7}$$

with

$$\epsilon(q,z) = (1 + 2\pi\,\alpha_{2\mathrm{D}}\,q)\cosh(zq) + [2 + 4\pi\,\alpha_{2\mathrm{D}}\,q\,(2\pi\alpha_{2\mathrm{D}}q)^2]\sinh(zq)/2\,. \tag{8}$$

In the above equations, $h = 6.9$ Å is the distance between the two layers, chosen as the distance between the planes parallel to the WTe_2 sheets passing through the W atoms, and z is the vertical coordinate. We set $z = 0$ ($z = h$) for intralayer (interlayer) interaction.

C. Excitons and spontaneously broken symmetry of the EI phase

The lowest exciton state for the GMS structure is plotted in the left column of Supplementary Fig. 2, the four contour maps in $\boldsymbol{k}$ plane corresponding to different vc pairs of the wave function component $\Psi_x^{vc\boldsymbol{k}}$. As clear from the colour map, the amplitude with the largest weight is $\Psi_x^{23\boldsymbol{k}}$ (third panel from top), which qualitatively overlaps with the modulus of the exciton wave function derived within the two-band model. The latter is shown in Fig. 3a of main text for finite y; the corresponding plot for $y = 0$ is qualitatively similar. The corrections introduced by the four-band model mainly consist in expanding the size of the Hilbert space that spans the exciton state, by means of adding wave function components. Note, though, that the weight of new components $\Psi_x^{vc\boldsymbol{k}}$ decreases with the increase of the e-h excitation energy for vc pair of bands located farther from Fermi energy. For the same reason, the maximum weight of $\Psi_x^{23\boldsymbol{k}}$ occurs in $\boldsymbol{k}$ space close to the position of the gaps separating bands 2 and 3.

Since the total momentum of the exciton is zero, the state must transform under symmetry operations according to the space group at Γ. It may be easily recognized from Supplementary Fig. 2 that the exciton wave function is even under the glide-mirror operation and odd under specular reflection (see for example the parity of e-h pairs at Γ). We checked that, for all $y \neq 0$, the lowest exciton state remains odd under reflection, whereas the glide-mirror symmetry is lifted by the sliding. This behavior rules the broken symmetry of the EI phase, since the noninteracting ground state wave function, which is even under specular reflection, is distorted by the hybridization with the (odd) exciton wave function at the onset of condensation [2]. It follows that the excitonic insulator must spontaneously break the mirror symmetry $x \to -x$, which is otherwise preserved in the absence of e-h attraction, for all y. This hints at "excitonic ferrolectricity" [3], which is driven by the macroscopic condensation of the interband exciton dipoles, here aligned along the x axis. Note that such exciton macroscopic dipole is orthogonal to the vertical macroscopic polarization that is observed experimentally. We expect the inclusion of spin-orbit coupling in the theory not to alter this picture, but possibly lead to additional symmetry breakings of magnetic type.

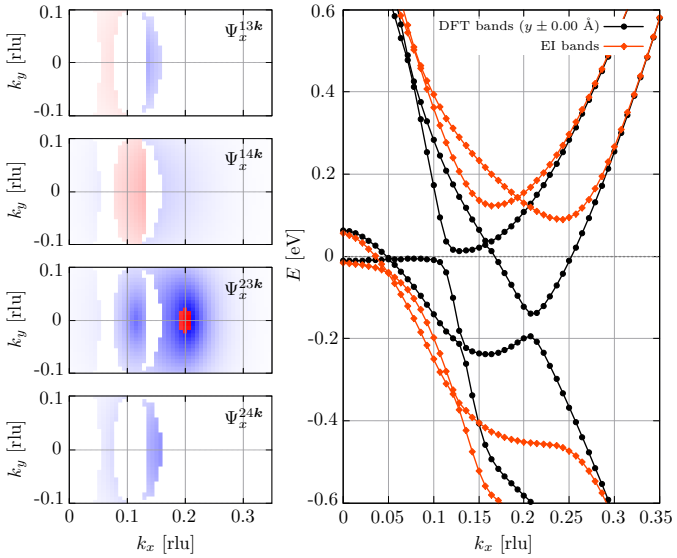

Supplementary Figure 2: **Bethe-Salpeter and EI gap equations within the four-band model.** Exciton wave function (left) and EI band reconstruction (right) within the four-band model for $\delta_{H_1} = 0$ (GMS structure). The panels on the left show the exciton wave function components, $\Psi_x^{vc\boldsymbol{k}}$, where $v = 1, 2$ and $c = 3, 4$ are the indices of the two valence and two conduction bands, in ascending order of energy. The range of the color scale is $[-0.1, 0.1]$, with positive [negative] values in red [blue]. As in Fig. 3 of the main text, the maximum amplitude is reached at the two locations along the ΓX cut of the energy gaps separating bands 2 and 3. The corrections to the bands in the EI phase, given by $\Delta_{ij}(\boldsymbol{k})$ (see main text), increase with the magnitudes of the amplitudes $\Psi_x^{vc\boldsymbol{k}}$. Note that, with respect to Fig. 3 of the main text, here the Brillouin zone sampling is reduced along the k_y direction. This significantly impacts the exciton binding energy, thus a lower screening ($\alpha_{2D} = 1.9$ Å) has been used to gap the EI band structure.

D. Self-consistent mean-field theory of the excitonic insulator

As for the two-band model illustrated in the main text, also in the present four-dimensional framework the EI ground state, $|\Psi_{\rm EI}\rangle$, is the Slater determinant of the filled, distorted valence band Bloch states,

$$|\Psi_{\rm EI}\rangle = \prod_{i=1,2} \prod_{\boldsymbol{k}} \hat{\alpha}^\dagger_{i\boldsymbol{k}} |{\rm vac}\rangle \,. \tag{9}$$

Here $|{\rm vac}\rangle$ is the vacuum state with no electrons, $\hat{\alpha}^\dagger_{i\boldsymbol{k}}$ is the Fermi operator that creates an electron of momentum $\boldsymbol{k}$ in the ith renormalized band of the excitonic insulator,

$$\hat{\alpha}_{i\boldsymbol{k}} = \sum_j a_{ij\boldsymbol{k}} \, \hat{a}_{j\boldsymbol{k}} \,, \tag{10}$$

$\hat{a}^\dagger_{j\boldsymbol{k}}$ creates an electron in the jth (conduction or valence) band of the pristine semimetal, and we convene that $i = 1, 2$ and $i = 3, 4$ respectively label the EI valence and conduction bands. The coefficients $a_{ij\boldsymbol{k}}$ occurring in (10) form a unitary matrix for given $\boldsymbol{k}$, which must be determined self-consistently. The $a_{ij\boldsymbol{k}}$'s are the eigenvectors resulting from the diagonalization of the mean-field Hamiltonian, $\hat{H}_{\rm EI}(\boldsymbol{k})$, the 4×4 matrix whose eigenvalues, $E_i(\boldsymbol{k})$, are the renormalized EI bands:

$$H_{\rm EI}(\boldsymbol{k}) = \begin{pmatrix} \varepsilon_1(\boldsymbol{k}) & 0 & \Delta_{13}(\boldsymbol{k}) & \Delta_{14}(\boldsymbol{k}) \\ 0 & \varepsilon_2(\boldsymbol{k}) & \Delta_{23}(\boldsymbol{k}) & \Delta_{24}(\boldsymbol{k}) \\ \Delta_{31}(\boldsymbol{k}) & \Delta_{32}(\boldsymbol{k}) & \varepsilon_3(\boldsymbol{k}) & 0 \\ \Delta_{41}(\boldsymbol{k}) & \Delta_{42}(\boldsymbol{k}) & 0 & \varepsilon_4(\boldsymbol{k}) \end{pmatrix} . \tag{11}$$

Here the pristine bands, $\varepsilon_i(\boldsymbol{k})$, are the eigenvalues of the noninteracting Hamiltonian, $\hat{H}(\boldsymbol{k}) = \hat{H}_0 + \hat{H}_1$ [see (2) and (3)], and the (real) self-consistent interband hybridization, $\Delta_{ij}(\boldsymbol{k}) = \Delta_{ji}(\boldsymbol{k})$, is driven by the population of the exciton condensate. This term, which generalizes to multiple bands the gap function $\Delta(\boldsymbol{k})$ discussed in the main text, must be determined by solving the "gap equation", which complements the iterative cycle:

$$\Delta_{ij}(\boldsymbol{k}) = \sum_{i',j',\boldsymbol{k}'} W^{i'j'\boldsymbol{k}'}_{ij\boldsymbol{k}} \sum_{l,l'} [a^{-1}_{\boldsymbol{k}'}]_{j'l} \, [a^{-1}_{\boldsymbol{k}'}]_{i'l'} \, \langle \hat{\alpha}^\dagger_{l\boldsymbol{k}'} \hat{\alpha}_{l'\boldsymbol{k}'} \rangle_{\Psi_{\rm EI}} \,. \tag{12}$$

Note that in (12)—and only there—the indices $i, i' = 1, 2$ and $j, j' = 3, 4$ run only over the valence and conduction states, respectively, $W^{i'j'\boldsymbol{k}'}_{ij\boldsymbol{k}}$ is given by (6), and the coefficients $[a^{-1}_{\boldsymbol{k}}]_{jl}$ are obtained by inverting the eigenvector matrix $a_{ij\boldsymbol{k}}$. We evaluate the quantum (and thermal) average $\langle \hat{\alpha}^\dagger_{l\boldsymbol{k}} \hat{\alpha}_{l'\boldsymbol{k}} \rangle_{\Psi_{\rm EI}}$ occurring in (12) as

$$\langle \hat{\alpha}^\dagger_{l\boldsymbol{k}'} \hat{\alpha}_{l'\boldsymbol{k}'} \rangle_{\Psi_{\rm EI}} = \delta_{l,l'} \, f[E_l(\boldsymbol{k})] \,, \tag{13}$$

where $f(\cdot)$ is the Fermi-Dirac distribution function. At zero temperature, for the intrinsic excitonic insulator phase, we set f to 1 for valence states and 0 for conduction states.

The numerical self-consistent cycle starts by using the components of the lowest-energy exciton, $\Psi^{ij\boldsymbol{k}}_x$, derived from the solution of the four-band Bethe-Salpeter equation (4), as a seed for $\Delta_{ij}(\boldsymbol{k})$ that enters the matrix (11). After $\hat{H}_{\rm EI}$ is diagonalized, the resulting orthogonal eigenvector matrix is inverted to evaluate the coefficients $[a^{-1}_{\boldsymbol{k}}]_{jl}$ entering (12). The new value of $\Delta_{ij}(\boldsymbol{k})$ is then inferred by performing the sum over $\boldsymbol{k}'$ in (12), and then used to update (11) at the next step. The cycle is repeated until $\Delta_{ij}(\boldsymbol{k})$ converges for all $\boldsymbol{k}$, i, j.

For completeness, we note that, in the presence of doping, or at finite temperature, or in the 'excitonic semimetal' scenario, the set of self-consistent equations reported above must be complemented by an additional condition, the total charge balance, which implicitly defines the chemical potential, μ. Such equation must be solved for μ at each step of the iterative cycle, as the chemical potential enters the average (13) through the Fermi distribution function. In principle, also the screened interaction W should be evaluated self-consistently, as the variation of μ impacts the screening of charge carriers [4]. In the simplest case of an intrinsic excitonic insulator at zero temperature, μ lies in the gap and the charge balance condition is unnecessary.

The method is illustrated in the right column of Supplementary Fig. 2, which compares the noninteracting and EI band structure for $\delta_{H_1} = 0$ and $\alpha_{\rm 2D} = 1.9$ Å, with a 50×29 $\boldsymbol{k}$-point grid. Note that the renormalization of the bottom conduction and top valence bands due to e-h interaction compares with that assessed within the two-band model, as shown in Fig. 3 of main text.

E. Discussion

The four-band model reported in this Supplementary Note provides valuable insight into the understanding of the variation of the band structure with y, the nature of the condensing exciton, and the consequent spontaneous breaking of the crystal symmetry. On the other hand, it has a few caveats, which we discuss in the following and that ultimately led us to present the two-band results in the main text.

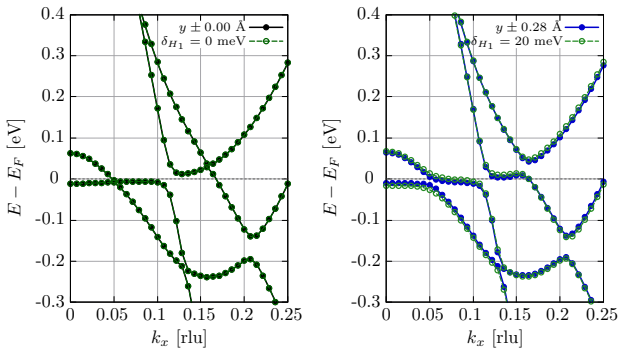

Supplementary Figure 3: **Comparison between model and first-principles bands.** Left: Model noninteracting bands, computed for $\delta_{H_1} = 0$ (open circles), compared to first-principles bands for the GMS structure, $y = 0$ (filled circles). Right: Model noninteracting bands, computed for $\delta_{H_1} = 20$ meV (open circles), compared to first-principles bands of the bilayer structure with the top layer displaced by ± 0.28 Å (filled circles). In both panels the bands are plotted along the ΓX cut of Brillouin zone ($k_y = 0$).

The first issue is the modeling of layer sliding through the envelope-function Hamiltonian $\hat{H}_1$ of (3), which does not depend on $\boldsymbol{k}$. A non-local, $\boldsymbol{k}$-dependent δ_{H_1} parameter would be needed to match exactly the evolution of band anticrossing with y, as predicted from density functional theory. This matter is illustrated in Supplementary Fig. 3. Whereas in the left panel the matching of first-principles (filled circles) and model (open circles) bands is complete by construction ($y = 0$), in the right panel ($y = \pm 0.28$ Å) the model conduction band crossing the Fermi energy around $k_x = (0.15)\, 2\pi/a$ overestimates the gap opening, while the valence band underestimates it. Though the discrepancy is tiny on the energy scale of the plot, the total energy gain associated with exciton binding is amplified by condensation, leading to a strong renormalization of the sliding barrier, as discussed in the main text.

Another concern is the envelope-function approximation at the basis of the four-band model, whose reliability deteriorates as one moves from the Brillouin zone center. The issue becomes severe for $|k_y| > (0.1)\, 2\pi/b$, due to the anticrossing behavior of bands that is not well reproduced by the model. This limits our ability to check the convergence of the solution of the Bethe-Salpeter equation (4) for large interaction strength. For this reason we relied eventually on the two-band model of the main text, based on energy bands purely derived from first principles, which allows us to extend arbitrarily the Brillouin zone sampling.

Reviewer 1: *Comment 2: The 2D polarizability α2D is a critical parameter for the Rytova-Keldysh potential (as shown in Supplementary Fig. 2). The value of 4.3 is used without justification. How was this value determined or estimated? A sensitivity analysis or a justification based on the electronic properties of bilayer WTe2 (e.g., from the DFT dielectric function) is essential to assess the robustness of the predicted gap and energy barrier.*

Authors Reply: We thank the reviewer for this pertinent recommendation. We have added a whole new Supplementary Section II in which we describe how the value of the two-dimensional polarizability $\alpha_{2\mathrm{D}}$ is determined. In the same section, we present an extensive analysis of the sensitivity of our results to the variations in $\alpha_{2\mathrm{D}}$ discussing the robustness of our results. In brief, we cannot compute $\alpha_{2\mathrm{D}}$ from our DFT calculations because the ground state is semimetallic, thus we set it to a value that results in the opening of a tiny many-body indirect gap that compares with the experiments. The extended discussion we added in the SI that addresses these points is reported below.

Reviewer 1: *Comment 3: How do we understand that Egap decreases with increasing α2D in Supplementary Figure 2?*

Authors Reply: (Please note that Supplementary Figure 2 which the Reviewer is referring to is now Supplementary Figure 5 in the updated version of the SI.) To clarify this point we added Supplementary Figure 4 in the SI. The figure shows how the exciton binding energy in our model for bilayer WTe_2 decreases with increasing $\alpha_{2\mathrm{D}}$. Lower exciton binding energy leads to smaller excitonic order parameters $\Delta_{ij}(\boldsymbol{k})$, which translates into smaller EI band renormalization and gap. An extended discussion is included in Supplementary Section II, reported below.

II. SENSITIVITY OF MODEL TO PARAMETERS AND VALIDATION FROM FIRST PRINCIPLES

Bilayer WTe_2 exhibits a tiny gap of a few meV, excitonic in nature [5], but is predicted to be a semimetal from DFT (Fig. 2 of main text). This poses a formidable computational challenge, since a full first-principles treatment of excitons would require the calculation of the GW correction to band structure, which includes dynamical screening effects, as well as the evaluation of the intraband contribution to electronic polarizability. Such high-level tasks are essential to capture excitonic effects in the presence of a two-dimensional Fermi surface [6–11]. Furthermore, the calculation of the EI phase is inherently self-consistent, in principle including the re-evaluation of screening at each step of the iterative cycle. This is relevant, as the static and dynamical GW correlations tend to decrease the semimetal band overlap and increase the range of the e-h attraction that binds excitons, which in turn may condense and open the gap. Eventually, the screening behavior of the reconstructed EI ground state is compatible with that of a narrow-gap semiconductor rather than that of the initial semimetal state.

Since the GW description of the bilayer is presently out of reach, we developed the two-band model approach of the main text. Luckily, two first-principles investigations recently reported consistent results for monolayer WTe_2 [5, 12], which we can use to validate the bilayer model, as we expect similar screening behaviour and exciton binding. Namely, Wu *et al.*, starting from a DFT semimetal ground state, showed [12] the tendency of the GW self-energy (in both flavors G_0W_0 and self-consistent COHSEX) to remove the Fermi surface by opening a gap. We expect a similar effect for the bilayer, which will tend to suppress the intraband contribution to screening. Importantly, the GW-corrected band structure by Wu *et al.* compares well with the one we derived previously (via hybrid DFT) to compute excitons from first principles [5]. Therefore, below we use the findings of Ref. 5 for the monolayer to benchmark those of the bilayer.

The two-band model critically relies on the parametrization of the screened e-h Coulomb attraction W via the polarizability α_{2D} [equation (3) of main text]. We cannot fix α_{2D} from the DFT calculation, since the predicted ground state is semimetallic: The occurrence of the spurious Fermi surface implies an intraband contribution to α_{2D}, which diverges at long wave length. The only consistent way to fix α_{2D} is to choose a value that results in the opening of a gap, which hence suppresses the intraband polarizability. Indeed, the chosen value of $\alpha_{2D} = 4.3$ Å provides a tiny many-body indirect gap that compares with experiments [5]. The resulting gap is 3 meV for $y = 0$ and 7 meV for $y = \bar{d}$ (Fig. 3b of main text, EI band structure).

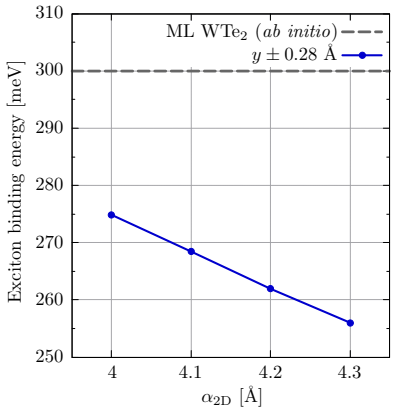

Supplementary Figure 4: **Exciton binding energy upon variation of the screening parameter.** Binding energy of the lowest exciton, resulting from the solution of Bethe-Salpeter equation (1) of main text, versus screening parameter α_{2D}. The results were obtained for sliding displacement $y \pm 0.28$ Å, using a 30×60 $\boldsymbol{k}$-point grid sampling the region $k_x \in [0, 0.3]$ rlu and $k_y \in [-0.3, 0.3]$ rlu. The lines connecting the dots are a guide to the eye. The dashed line highlights the exciton binding energy for monolayer (ML) WTe_2, computed from first principles [5].

We may justify further the chosen value of α_{2D} by contrasting the exciton binding energy inferred from W with the first-principle prediction for the monolayer [5]. This is illustrated in Supplementary Fig. 4, which compares the model exciton binding energy (dots) with the reference value [5] of 300 meV for the monolayer (dashed line), in the range $4 \leq \alpha_{2D} \leq 4.3$ Å. In general, as the screening of the e-h attractive potential increases with α_{2D}, the exciton binding energy decreases. Importantly, in the plotted range of α_{2D} the binding energy for the bilayer is smaller than the one for the monolayer, which matches the physical expectation of stronger screening in the bilayer. We disregard the outer

range of α_{2D}, since for $\alpha_{2D} \ll 4$ Å the bilayer binding energy nonphysically exceeds the monolayer value, whereas for $\alpha_{2D} > 4.3$ Å the resulting excitonic phase is semimetallic and the Rytova-Keldish form of W loses accuracy.

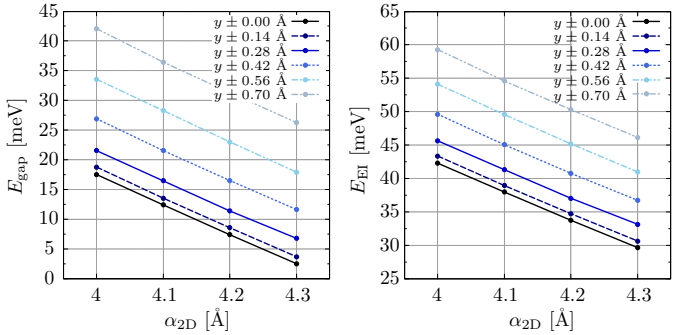

Supplementary Figure 5: **Energetics of the excitonic insulator vs screening and sliding displacement.** Many-body indirect gap in the EI phase, E_{gap} (left panel), and total energy gain, E_{EI} (right panel), versus screening parameter, α_{2D}, for various values of the sliding displacement, y. The connecting lines are a guide to the eye.

Like the exciton binding energy, also the EI gap function, $\Delta(\boldsymbol{k})$, converges to smaller values with increasing α_{2D}, which translates into weaker renormalization of EI bands and smaller size of the many-body indirect gap, E_{gap}. Remarkably, whereas E_{gap} is significantly sensitive to α_{2D}, the height of the sliding barrier potential is not. The reason is that the excitonic renormalization of the barrier height depends on the *variation* of E_{gap} with y, and not on its absolute magnitude. This is illustrated by Supplementary Fig. 5, which plots both E_{gap} (left panel) and the EI total energy gain, E_{EI} (right panel), vs α_{2D}, for different sliding displacements, y. Importantly, both curves are essentially parallel straight lines, namely, the variation of both E_{gap} and E_{EI} with y does not depend on the screening parameter, α_{2D}. In conclusion, the key result of our work, the excitonic renormalization of the height of the sliding barrier, is robust against the details of the two-band model.

Reviewer 1: *Comment 4: As far as I know, the ferroelectric switching barrier of different material is not related to the ferroelectric Curie temperature. For example, the ferroelectric sliding barrier is only a few meV in sliding ferroelectrics, but the FE order is stable at room temperature. Therefore, I do not think the author's simple estimate of 70 K is meaningful. Likewise, I don't understand the significance of the author's analogy with BCS model.*

Authors Reply: We do apologize for the sloppy formulation in the original manuscript. The Reviewer is obviously right, the intrinsic switching barrier does not directly determine the ferroelectric Curie temperature, as both intrinsic effects (like quantum and thermal fluctuations) and extrinsic effects (e.g. domain wall dynamics, defects, boundaries, etc) play a role. We have modified the text in both the Introduction and the final Discussion, to avoid the ambiguity signalled by the Reviewer.
At the moment, the first principles inclusion of extrinsic effects is out of reach. Our point is that, whatever these effects are, the impact of excitonic corrections on the energy barrier can be relevant.
Moreover, we have now removed the sentences discussing the analogy with BCS model.

Reviewer 1: *Comment 5: Could the authors discuss how exciton contributions affect sliding ferroelectric semiconductors?*

Authors Reply: We have added a whole new paragraph to the Introduction to discuss excitonic effects in 2D materials. This part reviews both the broad relevance of the excitonic insulator phase and the relation to other kinds of order, including ferroelectricity. The addition in the main text is reported below for convenience.

More generally, excitonic effects are widespread in 2D semiconductors and semimetals, due to enhancement of e-h correlations with reduced dimensionality [54, 55]. If the exciton binding energy exceeds the semiconductor gap size (or does not vanish in the semimetal), excitons may undergo Bose-Einstein condensation. This results into a new ground state, the EI [56, 57], which qualitatively differs from the pristine phase since a many-body gap opens [52, 53, 58–83], and/or a crystal symmetry is spontaneously broken [57–68, 84–86] (though concurrent lattice distortions spoil the EI picture in several candidate bulk materials [87–92]). The most fascinating aspect of the EI is the emergence of macroscopic quantum coherence [57, 93–98], which may appear e.g. as counterflow superconductivity, or anomalous enhancement of interlayer tunnelling, in bilayer systems with spatially separated electrons and holes [81–83, 94, 99–102]. An intriguing possibility is the 'excitonic ferroelectricity', where the macroscopic electric dipole arises from the coherent superposition of the interband electric dipoles associated with condensed excitons [64, 65, 93, 103] (see also Supplementary Section IC). Furthermore, excitons might trigger the transition to superconductivity upon a tiny amount of doping, like in the phase diagram of monolayer WTe_2 [104], mediate (unconventional) superconductivity [105–114] and magnetism [115, 116], and affect topological properties of 2D materials [64, 117].

Reviewer # 2

In this manuscript, the authors construct a model to investigate the impact of excitonic effects on the electronic structure and energy during the sliding process of WTe2 bilayers. Their results reveal that excitonic effects open a significant bandgap in WTe2 bilayers, leading the system to transition towards an excitonic insulator (EI) phase. This explains the experimentally observed Curie temperature, which is higher than predicted by density functional theory (DFT). While the work presents intriguing findings, several critical aspects require deeper exploration and substantial revisions to strengthen the manuscript for publication.

Reviewer 2: *1. When discussing the excitonic effect in the manuscript, the value $\alpha 2D$ = 4.3 Å appears. Could you please explain the origin of this data? Additionally, the text describes that $\alpha 2D$ = 4.3 Å opens a 3 meV energy gap in the energy band of GMS. Is this 3 meV energy gap reflected in the figure?*

Authors Reply: We have added a whole new Supplementary Section II in which we describe how the value of the two-dimensional polarizability α_{2D} is determined. In brief, we set it to a value that results in the opening of a tiny many-body indirect gap that compares with the experiments. The extended discussion in the SI is reported below. Regarding the energy gap, Figure 3b of main text shows the excitonic-insulator–induced band reconstruction for the bilayer structure with a sliding displacement of $y \pm 0.28$ Å, rather than for the GMS structure. Consequently, the gap shown in this figure is not 3 meV but 7 meV. This value is indeed reflected in the band structure and has now been explicitly stated in the figure caption to avoid confusion.

The two-band model critically relies on the parametrization of the screened e-h Coulomb attraction W via the polarizability α_{2D} [equation (3) of main text]. We cannot fix α_{2D} from the DFT calculation, since the predicted ground state is semimetallic: The occurrence of the spurious Fermi surface implies an intraband contribution to α_{2D}, which diverges at long wave length. The only consistent way to fix α_{2D} is to choose a value that results in the opening of a gap, which hence suppresses the intraband polarizability. Indeed, the chosen value of α_{2D} = 4.3 Å provides a tiny many-body indirect gap that compares with experiments [5]. The resulting gap is 3 meV for $y = 0$ and 7 meV for $y = \bar{d}$ (Fig. 3b of main text, EI band structure).

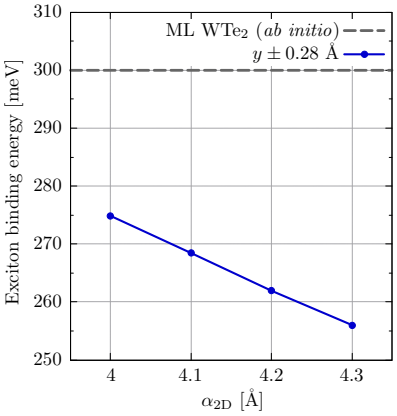

Supplementary Figure 4: **Exciton binding energy upon variation of the screening parameter.** Binding energy of the lowest exciton, resulting from the solution of Bethe-Salpeter equation (1) of main text, versus screening parameter α_{2D}. The results were obtained for sliding displacement $y \pm 0.28$ Å, using a 30×60 $\boldsymbol{k}$-point grid sampling the region $k_x \in [0, 0.3]$ rlu and $k_y \in [-0.3, 0.3]$ rlu. The lines connecting the dots are a guide to the eye. The dashed line highlights the exciton binding energy for monolayer (ML) WTe_2, computed from first principles [5].

We may justify further the chosen value of α_{2D} by contrasting the exciton binding energy inferred from W with the first-principle prediction for the monolayer [5]. This is illustrated in Supplementary Fig. 4, which compares the model exciton binding energy (dots) with the reference value [5] of 300 meV for the monolayer (dashed line), in the range $4 \leq \alpha_{2D} \leq 4.3$ Å. In general, as the screening of the e-h attractive potential increases with α_{2D}, the exciton binding energy decreases. Importantly, in the plotted range of α_{2D} the binding energy for the bilayer is smaller than the one for the monolayer, which matches the physical expectation of stronger screening in the bilayer. We disregard the outer range of α_{2D}, since for $\alpha_{2D} \ll 4$ Å the bilayer binding energy nonphysically exceeds the monolayer value, whereas for $\alpha_{2D} > 4.3$ Å the resulting excitonic phase is semimetallic and the Rytova-Keldish form of W loses accuracy.

Reviewer 2: *2. The manuscript mentions that the excitonic contribution is widespread in general two-dimensional systems. It is suggested to list the potential impacts of exciton in other studies to further reveal the research directions of excitonic effect in two-dimensional systems.*

Authors Reply: We thank very much the Reviewer for the suggested improvement of our manuscript. We have added a whole new paragraph to the Introduction that discusses excitonic effects in 2D materials. This part reviews both the broad relevance of the excitonic insulator phase and the relation to other kinds of order, including ferroelectricity. The addition in the main text is reported below for the sake of convenience.

More generally, excitonic effects are widespread in 2D semiconductors and semimetals, due to enhancement of e-h correlations with reduced dimensionality [54, 55]. If the exciton binding energy exceeds the semiconductor gap size (or does not vanish in the semimetal), excitons may undergo Bose-Einstein condensation. This results into a new ground state, the EI [56, 57], which qualitatively differs from the pristine phase since a many-body gap opens [52, 53, 58–83], and/or a crystal symmetry is spontaneously broken [57–68, 84–86] (though concurrent lattice distortions spoil the EI picture in several candidate bulk materials [87–92]). The most fascinating aspect of the EI is the emergence of macroscopic quantum coherence [57, 93–98], which may appear e.g. as counterflow superconductivity, or anomalous enhancement of interlayer tunnelling, in bilayer systems with spatially separated electrons and holes [81–83, 94, 99–102]. An intriguing possibility is the 'excitonic ferroelectricity', where the macroscopic electric dipole arises from the coherent superposition of the interband electric dipoles associated with condensed excitons [64, 65, 93, 103] (see also Supplementary Section IC). Furthermore, excitons might trigger the transition to superconductivity upon a tiny amount of doping, like in the phase diagram of monolayer WTe_2 [104], mediate (unconventional) superconductivity [105–114] and magnetism [115, 116], and affect topological properties of 2D materials [64, 117].

Reviewer 2: *3. The author discussed the influence of the excitonic effect on the band structure of bilayer WTe2 while neglecting SOC (Spin-Orbit Coupling). Could you please explain whether there is an interaction between the excitonic effect and SOC? Additionally, how would the band structure change if SOC is considered in the author's model?*

Authors Reply: We thank the referee for raising this point. We have added Supplementary Section III and Supplementary Figure 5 where we discuss the effects of SOC on both the DFT band structure and the excitonic insulator phase. In brief, while spin–orbit coupling modifies the detailed band structure and symmetry properties of the excitonic-insulator phase, it is not expected to qualitatively affect our main conclusions, which rely on the total excitonic energy gain as a function of the sliding displacement as we expect Rashba-like SOC contributions largely cancel when summing over occupied states. Still, a fully quantitative treatment of SOC-induced anticrossings would require a substantially more complex analysis beyond the scope of this work. We report the discussion here for ease of reference.

III. SPIN-ORBIT COUPLING

In the natural stacking of bilayer WTe_2 the inversion symmetry of the single-layer crystal structure is not preserved. As a result, spn-orbit coupling (SOC) splits the bands of bilayer WTe_2 by breaking Kramers degeneracy (Supplementary Fig. 6), while Bloch states remain doubly degenerate in monolayer WTe_2 [5]. Thus, the splitting effect must be attributed to inter-layer interaction, and may be tentatively rationalized as a Rashba-like term, $\sim \boldsymbol{S} \cdot (\boldsymbol{k} \times \boldsymbol{E})$, with $\boldsymbol{S}$ being the spin and $\boldsymbol{E}$ the microscopic electric field, after noting that the band splitting vanishes as $\boldsymbol{k} \to 0$ (right panel of Supplementary Fig. 6).

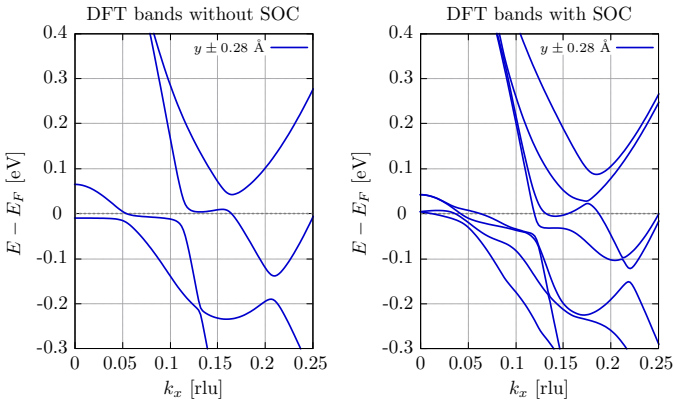

Supplementary Figure 6: **Effect of spin-orbit coupling on DFT bands.** DFT-PBE band structure without (left panel) and with (right panel) spin-orbit coupling (SOC). Results for the bilayer structure with sliding displacement $y \pm 0.28$ Å. The parameters of the DFT calculation with SOC are the same as in the Methods section of main text, with the exception that the corresponding full-relativistic pseudopotentials from the same library have been used [13].

Since our key findings depend on the variation of the total energy gain of the EI phase, $E_{\rm EI}$, with the sliding displacement y, we expect the inclusion of SOC not to alter qualitatively our conclusions. In fact, even if the energy bands split with the SOC field, we expect the Rashba-like corrections, $\sim \pm |\boldsymbol{k} \times \boldsymbol{E}|$, to substantially cancel out when summing over occupied states to compute $E_{\rm EI}$. An accurate statement would require to work out in detail the full numerical inclusion of SOC effects, as the intricacies of anticrossings shown in right panel of Supplementary Fig. 6 may compromise the reliability of any modelization. Such a task is beyond the scope of the present work.

On the other hand, SOC will qualitatively change the microscopic symmetries spontaneously broken by exciton condensation, as already mentioned in Supplementary Section I C. In particular, a magnetic instability could add to the breaking of the mirror symmetry $x \to -x$. The inclusion of SOC effects would significantly complicate the theory of the EI phase, by increasing the number of independent gap equations to solve self-consistently.

Reviewer 2: *4. In the experimental study of the sliding ferroelectricity of WTe2 bilayers, the properties of WTe2 bilayers at different temperatures were investigated. Is there an impact of temperature on the excitonic effect?*

Authors Reply: As shown in Supplementary Figure 4 (reported here below), the estimated exciton binding energy is more than 250 meV, much larger than the room temperature (T) energy scale. This implies that the overall excitonic renormalization of bands is robust against temperature, i.e., slowly decreasing with T below 300 K. On the other hand, the transport gap has indirect nature and is tiny. Therefore, even a small decrease of the energy-band renormalization will strongly affect transport properties, as seen in the experiments.

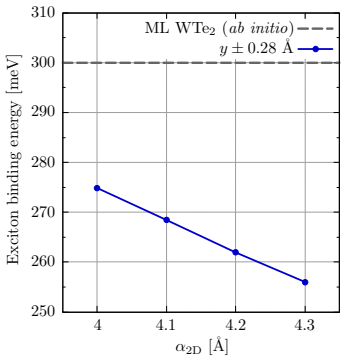

Supplementary Figure 4: **Exciton binding energy upon variation of the screening parameter.** Binding energy of the lowest exciton, resulting from the solution of Bethe-Salpeter equation (1) of main text, versus screening parameter α_{2D}. The results were obtained for sliding displacement $y \pm 0.28$ Å, using a 30×60 $\boldsymbol{k}$-point grid sampling the region $k_x \in [0, 0.3]$ rlu and $k_y \in [-0.3, 0.3]$ rlu. The lines connecting the dots are a guide to the eye. The dashed line highlights the exciton binding energy for monolayer (ML) WTe_2, computed from first principles [5].

Reviewer 2: *5. The manuscript employs a model to discuss the electronic properties of WTe2 bilayers under the excitonic effect. Have these properties been compared with other experimental or theoretical works? Could additional analysis be provided?*

Authors Reply: Comparison to other works and additional analysis is now provided in Supplementary Section II. The part concerning this point is reported below.

Bilayer WTe_2 exhibits a tiny gap of a few meV, excitonic in nature [5], but is predicted to be a semimetal from DFT (Fig. 2 of main text). This poses a formidable computational challenge, since a full first-principles treatment of excitons would require the calculation of the GW correction to band structure, which includes dynamical screening effects, as well as the evaluation of the intraband contribution to electronic polarizability. Such high-level tasks are essential to capture excitonic effects in the presence of a two-dimensional Fermi surface [6–11]. Furthermore, the calculation of the EI phase is inherently self-consistent, in principle including the re-evaluation of screening at each step of the iterative cycle. This is relevant, as the static and dynamical GW correlations tend to decrease the semimetal band overlap and increase the range of the e-h attraction that binds excitons, which in turn may condense and open the gap. Eventually, the screening behavior of the reconstructed EI ground state is compatible with that of a narrow-gap semiconductor rather than that of the initial semimetal state.

Since the GW description of the bilayer is presently out of reach, we developed the two-band model approach of the main text. Luckily, two first-principles investigations recently reported consistent results for monolayer WTe_2 [5, 12], which we can use to validate the bilayer model, as we expect similar screening behaviour and exciton binding. Namely, Wu *et al.*, starting from a DFT semimetal ground state, showed [12] the tendency of the GW self-energy (in both flavors G_0W_0 and self-consistent COHSEX) to remove the Fermi surface by opening a gap. We expect a similar effect for the bilayer, which will tend to suppress the intraband contribution to screening. Importantly, the GW-corrected band structure by Wu *et al.* compares well with the one we derived previously (via hybrid DFT) to compute excitons from first principles [5]. Therefore, below we use the findings of Ref. 5 for the monolayer to benchmark those of the bilayer.

Reviewer # 3

Excitons in TMDs have been known for a while. Connection with sliding ferroelectrics appears interesting. The manuscript by Rontani et al. reports the energy gain from exciton condensation in bilayer WTe2 and concludes that this condensation plays a critical role in stabilizing its sliding ferroelectricity. The data and logic presented are clear and accessible. However, the listed critical issues below must be satisfactorily addressed before I can reconsider my evaluation:

Reviewer 3: *1) Unlike in conventional bulk ferroelectrics, the calculated energy barrier separating two polarized structures does not serve as a definitive indicator of ferroelectric stability in sliding ferroelectrics. For example, bilayer BN—with an energy barrier of only 2 meV/f.u. remains stable well above room temperature (see Refs. 6 and 42), despite this barrier being significantly smaller than the thermal energy at 300 K. A continuum model from Bauer's group further suggests that WTe2 bilayers may exhibit a Curie temperature as high as 660 K with a sub-meV barrier (Phys. Rev. Lett. 130, 176801), which does not take exciton correction into consideration. Experimentally, stability can be strongly influenced by other factors such as boundaries, domain walls, etc. Thus, attributing the stability of sliding ferroelectricity in bilayer WTe2 observed in experiments primarily to exciton condensation lacks solid scientific justification.*

Authors Reply: We do apologize for the sloppy formulation in the original manuscript. The Reviewer is obviously right, the intrinsic switching barrier does not directly determine the ferroelectric Curie temperature, as both intrinsic (like quantum and thermal fluctuations) and extrinsic effects (e.g. domain wall dynamics, defects, boundaries, etc) play a role. We have modified the text in both Introduction and final Discussion, to avoid the ambiguity signalled by the reviewer. At the moment, the first principles inclusion of extrinsic effects is out of reach. Our point is that, whatever these effects are, the impact of excitonic corrections on the energy barrier can be relevant.

Reviewer 3: *2) According to the authors'data, the exciton binding energy is on the order of tens of meV, implying that exciton condensation can be readily disrupted and depopulated by thermal excitation at room temperature. It is therefore quite questionable to claim that excitons are responsible for the ferroelectric stability of bilayer WTe2 around room temperature.*

Authors Reply: As shown in Supplementary Figure 4 (reported below for the sake of convenience), the estimated exciton binding energy is more than 250 meV, much larger than the room temperature (T) energy scale. This implies that the overall excitonic renormalization of bands and sliding barrier is robust against temperature, i.e., slowly decreasing with T below 300 K. On the other hand, the transport gap has indirect nature and is tiny. Therefore, even a small decrease of the energy-band renormalization will strongly affect transport properties, as seen in the experiments.

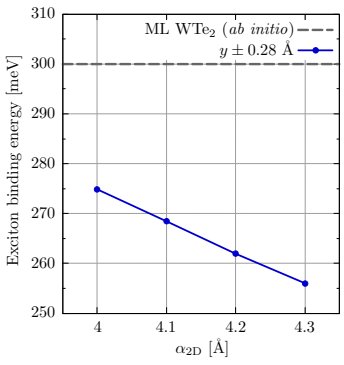

Supplementary Figure 4: **Exciton binding energy upon variation of the screening parameter.** Binding energy of the lowest exciton, resulting from the solution of Bethe-Salpeter equation (1) of main text, versus screening parameter α_{2D}. The results were obtained for sliding displacement $y \pm 0.28$ Å, using a 30×60 $\boldsymbol{k}$-point grid sampling the region $k_x \in [0, 0.3]$ rlu and $k_y \in [-0.3, 0.3]$ rlu. The lines connecting the dots are a guide to the eye. The dashed line highlights the exciton binding energy for monolayer (ML) WTe_2, computed from first principles [5].

Reviewer 3: *3) Figure 4 presents a corrected double-well potential profile. What are the polarization values at the corrected minima, and how well do they align with experimental measurements? Such comparison can make the data in the manuscript more convincing.*

Authors Reply: The value of the areal polarization density at the minima of the renormalized barrier is 2×10^4 e/cm, and we added it in the manuscript. This is, as expected, larger than the previous value of 1.5×10^4 e/cm but still compatible with the experimental one of 1×10^4 e/cm (both now reported in the manuscript).

Reviewer # 4

In their manuscript, D'Alessio et al. investigate the excitonic effects in sliding ferroelectric bilayer WTe2. They propose that (i) excitonic effects induce significant energy band renormalizations in the ground state, and (ii) exciton condensation helps stabilize ferroelectricity upon sliding, beyond previous predictions.

Reviewer 4: *Regarding point (i), the reported band renormalizations appear reasonable for bilayer WTe2, given its small bandgap. However, such effects may not be generalizable to other sliding ferroelectrics, such as MoS2, which possesses a larger bandgap.*

Authors Reply: The Reviewer is right that the energy band renormalization is relevant to the class of 2D materials that exhibit a narrow gap. We would like to emphasize that such class, which also includes semimetals, is broad and extremely interesting. The reason is that, in addition to band renormalization—an important effect by its own, exciton condensation is also related to a plethora of intriguing phenomena. These include the manifestation of macroscopic quantum coherence and the relation to other kinds of order (ferroelectricity, superconductivity, magnetism, possibly of unconventional kind). In order to convey this message to the broad readership of Nature Communications, we have now added an extended discussion in the Introduction, which we report below for convenience.

More generally, excitonic effects are widespread in 2D semiconductors and semimetals, due to enhancement of e-h correlations with reduced dimensionality [54, 55]. If the exciton binding energy exceeds the semiconductor gap size (or does not vanish in the semimetal), excitons may undergo Bose-Einstein condensation. This results into a new ground state, the EI [56, 57], which qualitatively differs from the pristine phase since a many-body gap opens [52, 53, 58–83], and/or a crystal symmetry is spontaneously broken [57–68, 84–86] (though concurrent lattice distortions spoil the EI picture in several candidate bulk materials [87–92]). The most fascinating aspect of the EI is the emergence of macroscopic quantum coherence [57, 93–98], which may appear e.g. as counterflow superconductivity, or anomalous enhancement of interlayer tunnelling, in bilayer systems with spatially separated electrons and holes [81–83, 94, 99–102]. An intriguing possibility is the 'excitonic ferroelectricity', where the macroscopic electric dipole arises from the coherent superposition of the interband electric dipoles associated with condensed excitons [64, 65, 93, 103] (see also Supplementary Section IC). Furthermore, excitons might trigger the transition to superconductivity upon a tiny amount of doping, like in the phase diagram of monolayer WTe_2 [104], mediate (unconventional) superconductivity [105–114] and magnetism [115, 116], and affect topological properties of 2D materials [64, 117].

Reviewer 4: *As for point (ii), the high Curie temperature can be adequately explained by molecular dynamics simulations using machine-learned force fields, which do not incorporate any excitonic effects.*

Authors Reply: We have now clarified in the manuscript, both in the Introduction and final Discussion, that our main aim is to highlight the role of excitons in renormalizing the sliding barrier. The effect is intrinsic and fundamentally relevant, irrespective of the explanation of the actual Curie temperature, which is in general complex and possibly related to extrinsic effects.

Reviewer 4: *While excitonic effects may play a role in narrow-gap or metallic sliding ferroelectric systems, I believe they are unlikely to be the key factor in stabilizing the ferroelectric state. Therefore, in my view, the manuscript in its current form may not be suitable for publication in Nature Communications.*

Authors Reply: Our revised manuscript clarifies the excitonic effect is present and relevant to a broad class of materials, as we argued above. We believe our findings may appeal the broad readership of Nature Communications.

List of changes

Here we list all the changes to the manuscript, following their order of appearance.

Changes to the main text:

- In the abstract we added "that disregard electron-hole interaction effects" after "beyond previous predictions".
- In the Introduction we changed "they are unable to account for the high Curie temperature observed in experiments" with "the accurate determination of the sliding energy barrier is still a challenge".
- In the Introduction we added a paragraph to highlight the broad interest evident from many works in the literature about many phenomena connected with exciton condensation.
- In the Results we added references to the SI, in particular: to Supplementary Section III when we mention spin-orbit coupling effects; to Supplementary Section I and Supplementary Fig. 1 when we mention the four-band model; to Supplementary Section II when we introduce the value of α_{2D}; to Supplementary Fig. 4 when we comment on the value of the exciton binding energy.
- In the Results we removed the sentence "the estimated energy barrier does not clarify how this material can retain its ferroelectric properties at high temperatures" and added "This hints at a polarization density and energy barrier higher than predicted, as DFT overestimates the electronic screening".
- We slightly modified the caption of Fig. 3 indicating the model parameters at the beginning and adding the value of the EI band gap. We also modified the key of the graph adding the value of sliding displacement corresponding to the plotted bands.
- In the Results we removed the value in K of the renormalized barrier.
- In the Results we added the value of the areal polarization density at the minima of the renormalized barrier as well as the experimental estimate of the same quantity.
- In the Results we removed the paragraph concerning the analogy with the BCS theory.
- In the Discussion we added a reference to Supplementary Section II when we mention the robustness of our results upon changing the value of α_{2D}.
- Discussion we added the sentence "This will add to other effects, both intrinsic (intralayer stiffness, vdW interaction, quantum and termal fluctuations) and extrinsic (e.g. domain wall dynamics, defects, boundaries, etc), dictating the Curie temperature and switching properties of the system" to contextualize our main result.
- In the Methods we corrected the convergence threshold on forces and added the value of the plane wave expansion cutoff we used for NEB calculations.
- In the Methods we added the citation to the Zenodo page where the code and data to reproduce the results can be found.
- We corrected the units and added all the sections required to comply with the Nature Communications formatting instructions.

Changes to the Supplementary Information:

- We added the details of the four-band model and excitonic insulator model in Supplementary Section I, including a new Supplementary Fig. 1.
- Supplementary Fig. 1 of the previous version is now Supplementary Fig. 2. We added the value of sliding displacement corresponding to the plotted bands in the key of the graph and slightly changed the caption.
- We added Supplementary Fig. 3 to show the comparison between the four-band model and the DFT bands.
- We added Supplementary Section II, which includes: a discussion on how we determine the value of α_{2D} that we use in the main text; a comparison with other works on WTe_2 in the literature; comments on the robustness of our results upon changing α_{2D}.

- We added Supplementary Fig. 4 to show how the exciton binding energy decreases when increasing α_{2D}, together with a paragraph in Supplementary Section II which clarifies how E_{gap} decreases with increasing α_{2D}.
- Supplementary Fig. 2 of the previous version is now Supplementary Fig. 5, and part of its previous caption has been moved in the text of Supplementary Section II.
- We added Supplementary Section III and Supplementary Fig. 5 to comment the effects of SOC on the DFT band structure.

Reply to reviewers

March 9, 2026

We thank Reviewers very much, for their constructive criticisms as well as for the time spent in the review process. In the following, we address all the remaining comments, by Reviewer # 1 and # 3, point by point. We believe that the insights and suggestions by all Reviewers have been essential to strengthen the paper and sharpen its focus and motivation.
For ease of reference we reproduce here the review reports in *Italics*. Our responses are in Roman font. The new changes in the main manuscript are highlighted in red, while those resulting from the previous review have been integrated with the text in black.

Reviewer # 1

The author's response generally addressed my concerns. I believe this work is important for understanding the sliding ferroelectric problem in narrow-bandgap (or semimetallic) layered materials, and its conclusions are appropriate; therefore, I recommend the paper be accepted.

The author provided details about the method and offered code for verification, greatly enhancing the reproducibility. In the end, before publication, please add the details on how to obtain the "phonon" parameter δ_{H1} via "y" in the the supplementary materials.

Authors Reply: We thank Reviewer # 1 very much for all past and present insightful suggestions, which—we believe—helped us to substantially improve the manuscript.

We added the details on how to obtain the value of δ_{H_1} in Supplementary Section IIE. For ease of reference, we include here the related paragraph.

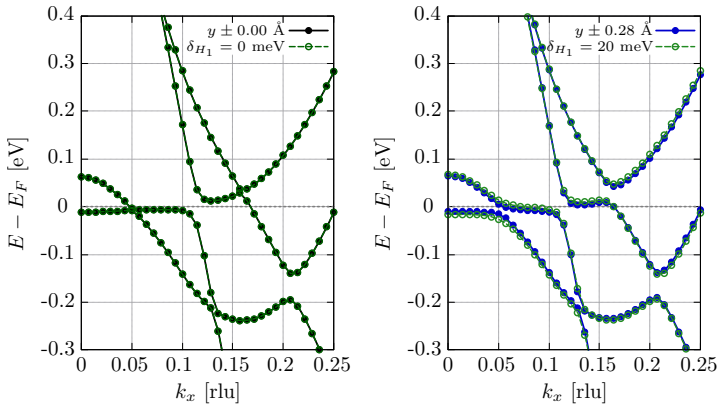

Supplementary Figure 5: **Comparison between model and first-principles bands.** Left: Model noninteracting bands, computed for $\delta_{H_1} = 0$ (open circles), compared to first-principles bands for the GMS structure, $y = 0$ (filled circles). Right: Model noninteracting bands, computed for $\delta_{H_1} = 20$ meV (open circles), compared to first-principles bands of the bilayer structure with the top layer displaced by ± 0.28 Å (filled circles). In both panels the bands are plotted along the ΓX cut of Brillouin zone ($k_y = 0$).

The first issue is the modeling of layer sliding through the envelope-function Hamiltonian $\hat{H}_1$ of (3), which does not depend on $\boldsymbol{k}$. This simplification allows for assessing the "frozen phonon" parameter, δ_{H_1}, by maximizing the overlap with the target DFT bands computed for a given sliding displacement. For example, for ± 0.280 Å displacement of the top layer from the GMS structure, we find $\delta_{H_1} = 20$ meV (right panel of Supplementary Figure 5). However, a non-local, $\boldsymbol{k}$-dependent δ_{H_1} parameter would be needed to match exactly the evolution of band anticrossing with y, as predicted from density functional theory. This matter is illustrated in Supplementary Fig. 5. Whereas in the left panel

Reviewer # 2

Having reviewed the reply, I accept the paper for publication in its current form.

Authors Reply: We thank Reviewer # 2 very much for the careful assessment of our paper and constructive suggestions. We acknowledge that the Reviewer's previous report was instrumental to strengthen our paper.

Reviewer # 3

After carefully considering the authors' responses, the central concern raised in the original review remains unresolved. As I understand it, the claimed novelty of the manuscript—as suggested by its title—rests on the assertion that exciton condensation induces a substantial renormalization of the interlayer sliding barrier in bilayer WTe_2, thereby enabling robust sliding ferroelectricity at room temperature. This claim is motivated by the fact that, in the absence of excitonic effects, the intrinsic sliding barrier is on the sub-meV scale. However, neither the revised manuscript nor the authors' responses provide convincing or quantitative evidence to substantiate this proposed mechanism. As emphasized in the previous review, the magnitude of the sliding barrier enhanced by exciton condensation is not a determining factor for the existence or stability of sliding ferroelectricity itself. Instead, it is primarily an indicator of the switching characteristics under an external electric field. Existing experimental and theoretical studies have already established that sliding ferroelectricity in WTe_2 is highly robust at and below room temperature, despite the intrinsically small (sub-meV) barrier. The excitonic effect in this material is not as important as claimed in the stabilization of ferroelectricity. Furthermore, the influence of exciton condensation is expected to be relevant only at low temperatures. Although the exciton binding energy in WTe_2 is relatively large (on the order of 270 meV), exciton condensation has been reported to occur at much lower temperatures, around 100 K (see, e.g., Refs. 52 and 53). This significantly limits the temperature window in which excitonic effects can meaningfully contribute to the ferroelectric behavior, particularly at/near room temperature. Given these considerations, the overall scientific contribution of the manuscript requires reassessment. In its present form, the work does not convincingly demonstrate a level of novelty or impact commensurate with the standards required for publication in Nature Communications.

Authors Reply: We would like to thank Reviewer # 3 very much for carefully thinking about our manuscript and providing insightful advise, which helped us to strengthen our work, including sharpening its focus and motivation. We fully address all the criticisms in the following.
Please note that Refs. 52 and 53 mentioned by the reviewer are now Refs. 54 and 55 in the updated version of the manuscript.

In brief, Reviewer # 3 raises two criticisms that affect the novelty and impact of our work: (1) The sub-meV magnitude of the sliding barrier, as derived by DFT-NEB method, is alone sufficient to explain the stability of ferroelectricity up to ≈ 300 K. (2) Excitonic effects are relevant only below ≈ 100 K.

(1) DFT magnitude of the sliding barrier. We have carefully reconsidered our DFT-NEB estimate of the sliding barrier, taking special care of extrapolation to zero electronic temperature. Our well converged results point to a barrier height of ≈ 0.1 meV, significantly smaller than previous predictions [one third with respect to Liu *et al.*,, Nanoscale **11,** 18575 (2019); one sixth with respect to Yang *et al.,* JPCL **9,** 7160 (2018), and Bai *et al.,* Nature Commun **16,** 7221 (2025)]. Consistently with our new estimate, the thermodynamic mean-field theory by Tang and Bauer [PRL **130,** 176801 (2023)] predicts a Curie Temperature (T_c) of ≈ 330 K, half the original prediction for WTe_2. As two-dimensional quantum fluctuations significantly suppress the mean-field T_c magnitude (e.g., in the Ising square lattice they almost halve it), it is unclear whether the bare sliding barrier alone explains the observed ferroelectric order, i.e., its stability and switching properties up to room temperature.

Apart from our numerical result, we would like to emphasize the fundamental aspect of our finding, which we ascribe to the presence of a Fermi surface in bilayer WTe_2 (in the absence of excitonic effects). As already pointed out by Reviewer # 3 in the previous report, the large magnitude of T_c is generically explained by the macroscopic mass associated with layer sliding dynamics [Tang and Bauer, PRL **130,** 176801 (2023)], i.e., the rigidity (incompressibility) of the layers. For a large gap semiconductor, like h-BN, both lattice and electron liquid are incompressible, leading to high T_c, and we expect the DFT-NEB barrier not to change for decreasing electronic temperature (nor we expect relevant excitonic effects). On the other hand, the electron liquid of the semimetallic bilayer WTe_2 is highly compressible. As we demonstrate in the newly added Supplementary Section I, the high electron compressibility suppresses T_c, through the reduction of the sliding barrier height for $T \to 0$. Exciton condensation opens a bandgap and makes the electron system incompressible, similarly to the h-BN paradigm.

The above points are now discussed in the introductory part of the main text, whereas full details are provided in the newly added Supplementary Section I. We report below the changes for the ease of Reviewer # 3.

I. ESTIMATE OF THE DFT-NEB FERROELECTRIC SWITCHING BARRIER

In this section we apply the nudged elastic band (NEB) method, as implemented in the DFT framework [1], to estimate the energy barrier of the sliding ferroelectric switching. We take special care of exploiting the Fermi-Dirac occupation function to account for the electronic temperature through the smearing parameter, and discuss how this impacts the NEB energy barrier, as well as the DFT band structure.

In the following we report results for a smearing parameter decreasing from 5×10^{-3} Ry (i.e., ≈ 800 K) down to 5×10^{-4} Ry (≈ 80 K). Though 800 K may look like a large value, this is the typical order of magnitude used to speed up the convergence of the self-consistent DFT calculation, particularly when dealing with a coarse $\boldsymbol{k}$-point sampling of the Brillouin zone combined with a Fermi-Dirac occupation function. As a lower smearing parameter requires a denser Brillouin-zone sampling to achieve numerical convergence, we increased the $\boldsymbol{k}$-point grid from 22×12 to 66×36, which yields fully converged results.

Furthermore, as the interplay between $\boldsymbol{k}$-point density and the smearing parameter influences the equilibrium configuration through the evaluation of forces, we performed variable-cell relaxations to optimize both the atomic positions and the lattice parameters for each given combination of smearing parameter and $\boldsymbol{k}$-point grid.

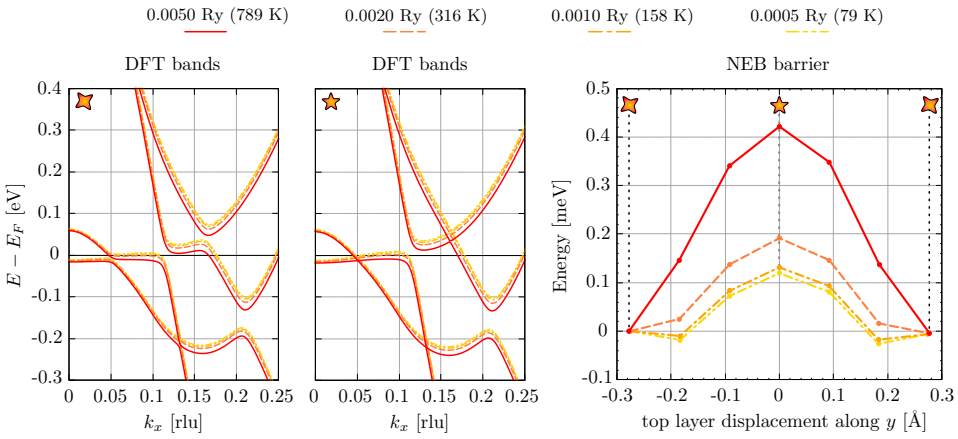

Supplementary Figure 1: **DFT and NEB results at different electronic temperatures.** DFT band structures of bilayer WTe_2 (left and center panels) and NEB energy barrier of the sliding ferroelectric switching (right panel) using a 66×36 **k**-point grid for the different smearing parameters reported on top. The smearing parameter fixes the electronic temperature through the Fermi-Dirac occupation function. The band structures in the left panel correspond to the equilibrium configuration obtained via variable-cell relaxation (diamond symbol), whereas those in the center panel to the glide-mirror symmetric (GMS) structure found by the NEB calculation (star symbol). In the left and center panels the bands are shifted by their respective Fermi energy, whereas in the right panel each NEB curve is shifted so that its first image (i.e. the starting configuration of the reaction path) is at zero energy. The values on the horizontal axis of the right panel correspond to the relative sliding displacement between the layers, with zero displacement corresponding to the GMS configuration. The circles on the NEB curves mark the images used for the discretization of the reaction path, and the connecting lines are a guide to the eye.

As shown in the left and center panels of Supplementary Figure 1, the smearing parameter changes the DFT band structure—already converged for a 22×12 grid—without affecting the magnitude of the gaps at $k_x \approx 0.12$ rlu and $k_x \approx 0.21$ rlu. Therefore, our results for the excitonic renormalization of the switching barrier, presented in the main text, are unaffected. However, the smearing parameter strongly affects the occupation of valence states for $0.05 < k_x < 0.12$ rlu, which are filled only for temperatures higher than ≈ 300 K. This band region is remarkably flat not only along k_x but also along k_y (cf. Supplementary Figure 3c), hence providing a sizable contribution to the density of states in the Fermi energy window. Similarly, a significant enhancement of the density of states originates from the conduction band for $0.12 < k_x < 0.17$ rlu, though at higher temperature and sliding displacement (cf. Figure 2 of the main text).

The above behavior points to a wide variation of Gibbs free energy (the extensive counterpart of the chemical potential) with temperature, and reflects in the extreme sensitivity of the NEB potential barrier to the smearing parameter. This is illustrated in the right panel of Supplementary Figure 1, where the energy zero for each curve is

fixed to the energy of the respective starting configuration. For given layer displacement coordinate, the NEB energy potential increases with the smearing parameter, the maximum variation corresponding to zero displacement (GMS structure). This may be easily rationalized, as the valence band of the GMS configuration is almost perfectly flat for a significant k_x range (center panel of Supplementary Figure 1), and hence its filling is most sensitive to temperature.

This results in a general reduction of the switching barrier with decreasing temperature. The trend shown in the right panel of Supplementary Figure 1 suggests that, at zero temperature, the barrier stabilizes to a value around 0.1 meV. The barrier "width"—the horizontal sliding displacement that connects the two ferroelectric ground states with opposite dipole—shows a similar trend, i.e., it shrinks as the electronic temperature is lowered.

The barrier height values previously published were obtained with the same methodology but were significantly higher: 0.6 meV [2, 3] and 0.3 meV [4]. We note that in those works smaller $\boldsymbol{k}$-point grids were used. In conclusion, the huge suppression of the NEB potential barrier height we report may be ascribed to the very high value of the electronic density of states at Fermi energy, i.e., the extreme compressibility of Fermi liquid. We expect no such effect for the incompressible Fermi system of a large-gap semiconductor, like h-BN.

Interestingly, the increase in the switching barrier with temperature was recently measured (above 100 K) in bilayer WTe_2 and attributed to the appearance of the Fermi surface [3]. The experiment might be related to the results reported in the main text, as the predicted excitonic indirect gap varies between 3 meV ($\approx$ 35 K, GMS structure) and 7 meV ($\approx$ 80 K, $\bar{d}$ displacement) with sliding.

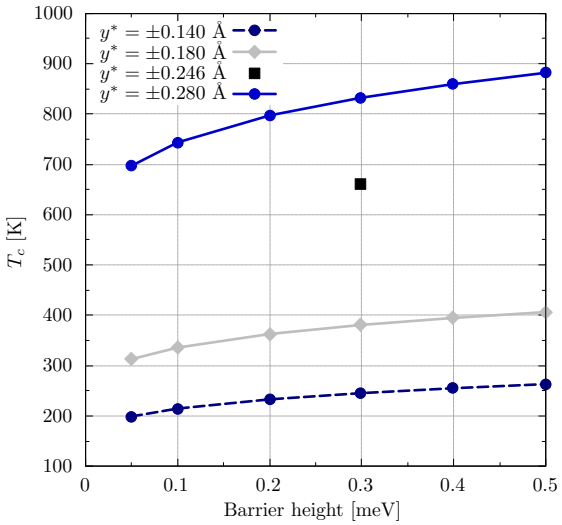

Supplementary Figure 2: **Ferroelectric switching Curie temperature (T_c) after Tang and Bauer (2023).** The plot reports the numerical solution of equation (19) of Ref. 5. Here y^* is used to indicate the relative sliding displacement between the GMS configuration and the minimum energy configuration (i.e., half the NEB barrier width). The black square points to the estimate for bilayer WTe_2 given in Ref. 5. The other curves are estimates of T_c for both larger and lower values of barrier height and width, for a range of values relevant to the NEB barrier results of Supplementary Figure 1. The connecting lines are a guide to the eye.

According to the thermodynamic mean-field theory of Ref. 5, the key to the high Curie temperature (T_c) of sliding ferroelectrics is the rigidity of the layer sliding, which proceeds with a macroscopic mass. In addition to structural parameters (unit cell area and the 2D Lamé coefficients), presumably unchanged in our treatment with respect to the values reported in Table I of Ref. 5, T_c is most sensitive to the switching barrier height and width, as shown in Supplementary Figure 2. From Supplementary Figure 1 we estimate a barrier height of $\approx$ 0.1 meV and width $y^* \approx 0.180$ Å, leading to $T_c \approx 330$ K, which is half the original prediction for bilayer WTe_2 (black square dot [5]). As the mean-field treatment of the layer sliding dynamics is known to overestimate T_c by neglecting quantum fluctuations, it remains unclear whether the DFT treatment alone is able to explain the room-temperature ferroelectricity of bilayer WTe_2. This uncertainty points to the relevance of the excitonic enhancement of the switching barrier height discussed in the main text.

charge transfer compatible with the measured polarization [2, 48], the accurate determination of the sliding energy barrier is still a challenge ~~an issue of relevance in view of room-temperature operation, as also discussed in Refs.~~ [49–51]: an issue especially relevant for the room-temperature operation of ferroelectric semimetals.

For ferroelectric semiconductors, like h-BN, the tiny potential barrier ($\sim$ 2 meV) is sufficient to stabilize ferroelectricity, since both lattice and electrons are rigid and slide with macroscopic mass [49]. For ferroelectric semimetals, the electron system is compressible [52] and reacts to sliding (Supplementary Section I). As a consequence, the sliding barrier is reduced by at least one order of magnitude ($\sim$ 0.1 meV, see Supplementary Figure 1). The suppression of the barrier, which was not appreciated by previous work (DFT estimates of Refs. 2, 48, and 53 were significantly larger), calls into question the actual origin of the ferroelectric order, its stability and switching properties.

Here we move from the recent evidence of important excitonic effects in mono- and bi-layer WTe_2, leading to a ground-state excitonic insulator (EI) phase [54, 55],

(2) Excitonic effects above $\approx$ 100 K. We would like to emphasize that the available experimental evidence shows that the critical temperature of the excitonic insulator phase in monolayer WTe_2 is *at least* of the order of 100 K. Such lower bound is inferred from a combination of transport experiments, mainly the measurement of the chemical potential, μ, as the monolayer is doped through electrostatic gating. The relevant experimental dataset by Sun *et al.*, Nature Physics **18,** 94 (2022), is included in Reply Figure 1(b) for the sake of convenience. The key evidence is the step-like behavior of μ at charge neutrality, which remains clearly visible up to $\approx$ 100 K. It is important to stress that the smearing of the step at higher temperature does not rule out the survival of macroscopic coherence, since the blurring of $\Delta\mu$ is due to the thermal excitation of quasiparticles, which occurs even in the presence of a many-body gap.

We recently developed a self-consistent quantitative theory of the excitonic insulator phase in monolayer WTe_2, which builds on first principles and deals with the effects of strong spin-orbit coupling, as well as it includes the spin and valley degrees of freedom of the condensate [Cardoso *et al.,* manuscript to be published (2026)]. The predicted doping behaviour of μ [Reply Figure 1(a)] agrees well with the measured one [Reply Figure 1(b)], and is consistent with a critical temperature falling in the range 350-400 K.

The effect of the temperature on the condensate is best appreciated in Reply Figure 2, which shows the (folded) band structure of the excitonic insulator, both below and above 100 K. Importantly, as the temperature raises the excitonic indirect band gap is reduced but remains finite up to at least 350 K. For larger temperature, the bands collapse into the pristine DFT structure (dashed curve), i.e., the band structure in the absence of excitonic effects.

In conclusion, on a theoretical basis we expect the excitonic insulator phase to survive well above room temperature in monolayer WTe_2. We are unable to predict the critical temperature of the bilayer, as a reliable estimate requires a first-principles calculation beyond the DFT level, which is presently on the verge of our computational capability. On the other hand, on a physical basis we expect the critical temperature of the bilayer to be smaller but comparable to the one of the monolayer.

Overall, the above arguments—though mainly theoretical—point to the potential role of the excitonic renormalization of the sliding barrier in stabilizing the ferrolectric phase of bilayer WTe_2, below and at room temperature. We hope Reviewer # 3 may agree on this statement. We believe our findings are sufficiently relevant to appeal the broad readership of Nature Communications.

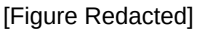

Reply Figure 1: **Chemical potential vs gated charge density for monolayer WTe_2.** Predicted (a) and measured (b) chemical potential, μ, vs gated charge density, n_g, for different temperatures, T. The measured data for $T < 10$ K are unpublished and for $T \geq 10$ K are taken from Sun *et al.*, Nature Physics **18,** 94 (2022). The predicted values are obtained by the self-consistent mean-field theory of the EI phase, which fully takes into account the first-principles band structure, spin-orbit interaction, spin and valley degrees of freedom. After Cardoso *et al.,* manuscript to be published (2026).

Reply Figure 2: **Predicted temperature dependence of the excitonic insulator (EI) band structure of monolayer WTe_2.** The EI critical temperature is between 350 and 400 K. The dashed curves are DFT energy bands, computed in the absence of excitonic effects (conduction bands are folded at Γ). EI bands are obtained by setting the polarizability to match predicted and measured band gap (here the predicted indirect gap is 43 meV). The EI band structure is obtained by the self-consistent mean-field theory of the EI phase, which fully takes into account the first-principles band structure, spin-orbit interaction, spin and valley degrees of freedom. After Cardoso *et al.,* manuscript to be published (2026).

Reviewer # 4

I have read the authors' reply. It seems my understanding on the manuscript is right. The novelty of this manuscript is to propose "exciton effects renormalize the sliding barrier". I think it does not play the key role in the stabilizing the ferroelectricity. Nevertheless I cannot judge whether the novelty and importance meet the standard of Nat. Comm. or not; I therefore suggest the editor to find one more referee to judge its novelty and importance.

Authors Reply: We thank Reviewer # 4 very much for the careful reading of our paper and helpful comments, though we respectfully disagree about the relevance of the excitonic renormalization of the sliding barrier. This point has been explicitly clarified in the revised manuscript and discussed in detail in our response to Reviewer # 3.

List of changes

Here we list all the changes to the manuscript, following their order of appearance.

Changes to the main text:

- We added a paragraph in the Introduction to address the points raised by Reviewer # 3. The paragraph also refers to the new Supplementary Section I, which presents a more detailed discussion complete with new data.
- In the Results we clarified the comparison between our calculation of the sliding barrier with previous theoretical works in light of the new results.
- We updated all the references to Supplementary Sections and Figures throughout the main text following the changes to the Supplementary Information.

Changes to the Supplementary Information:

- We added new data on the dependence of DFT and NEB results on electronic temperature in a new Supplementary Section I, which also includes two new figures (Supplementary Figures 1 and 2).
- Supplementary Sections I, II, III of the previous version are now Supplementary Sections II, III, IV respectively.
- Supplementary Figures 1, 2, 3, 4, 5, 6 of the previous version are now Supplementary Figures 3, 4, 5, 6, 7, 8 respectively.
- We added the details on how to obtain the value for the δ_{H_1} parameter in Supplementary Section IIE.